Large growth rate instabilities in three-layer flow down an incline in the limit of zero Reynolds number

Steven J. Weinstein
Eastman Kodak Company, Rochester, New York 14652-3701

Kang Ping Chen
Department of Mechanical and Aerospace Engineering, Arizona State University, Tempe, Arizona 85287-6106

(Received 29 December 1998; accepted 21 July 1999)

In this paper, we examine the effect of viscosity stratification on wave propagation in three-layer flow down an inclined plane at vanishingly small Reynolds number and at finite wavelengths, for cases of negligible liquid–liquid interfacial tensions. We have found that the long-wavelength interface mode inertialess instability of Weinstein and Kurz [Phys. Fluids A **3**, 2680 (1991)] persists into the finite wavelength domain in the form of nearly complex conjugate wave speed pairs; in certain limits, the interface modes are precisely complex conjugates. As in the case of Weinstein and Kurz, the physical configuration necessary to achieve inertialess instability is a low viscosity and thin internal layer with respect to the other layers in the film. The largest growth rate of the inertialess instability is found at finite wavelengths on the order of the total thickness of the film, and is orders of magnitude larger than the maximum growth rates identified by Lowenhurz and Lawrence [Phys. Fluids A **1**, 1686 (1989)] for two-layer flows. We have also found an additional configuration exhibiting extremely large growth rates, also characterized by nearly complex conjugate behavior, that is not accessible via a long or short wavelength asymptotic limit; these three-layer structures have thin, high viscosity internal layers. The characteristic wavelengths associated with the largest growth rates are on the order of ten times smaller than those for the low viscosity internal layer cases. The influence of the deformable free surface on the growth rates of these interface modes is studied and found to be significant. © *1999 American Institute of Physics.* [S1070-6631(99)01511-1]

I. INTRODUCTION

The rectilinear flow of fluid layers down an incline is a configuration often found in the manufacture of multiple-layer products such as photographic films. The inclined surfaces of a coating die provide the means by which laminar liquid layers can be stacked on top of one another, in preparation for subsequent coating onto a moving substrate. Immediately after application on the substrate and prior to drying (which creates a final solid product), the liquid layers are mobile, and if the substrate is configured such that it is nonhorizontal (which may happen because of some mechanical constraint on a process), gravity induces a flow with respect to the substrate. When viewed in a frame of reference moving with the substrate, this velocity field is again rectilinear incline flow. It is well known that incline plane flows exhibit flow instabilities, in the form of traveling waves, that create undesirable thickness variations in the multiple layer coating structures.

There is an extensive literature on the stability and growth of waves on inclined liquid films (e.g., Joseph and Renardy[1] and Chen[2]). Of relevance to the current work is the role of fluid inertia in the linear stability of Newtonian incline flows. For a given layer in the flow, inertia is quantified by the Reynolds number, $\mathrm{Re}=\rho Q/\mu$, where ρ, Q, and μ are the density, volumetric flow rate per unit width, and viscosity. For single-layer systems, fluid inertia, i.e., $\mathrm{Re}\neq 0$, is required to induce finite wavelength instabilities (Benjamin,[3] Yih[4]); regardless of the amount of inertia, single-layer flows are neutrally stable in the limit of infinitely long wavelength disturbances. Single-layer instabilities are typically surface modes, and owe their existence to the presence of a deformable air–liquid interface. Shear mode instabilities can also arise (i.e., Tollmien–Schlichting waves) but they are relevant only at extremely low angles of inclination and at high Reynolds numbers.[5,6]

In Newtonian systems with a distinct difference in fluid properties (density or viscosity) between layers, the number of wave solutions is equal to the number of interfaces in the system at moderate Reynolds numbers.[7–9] All wave solutions must be stable for a given fluid system to be stable. In multiple-layer flows, one of the wave solutions has properties that are similar to that in the single-layer system, and in fact, persists in the limit as the layer properties become similar; for this reason, it is called a surface mode. The remaining wave solutions are referred to as interface modes. Each interface mode owes its existence to a jump in liquid properties across a specific interface in the multiple-layer structure. As in single-layer systems, the surface mode requires inertia to exhibit wave growth when there are multiple layers.[10] However, interface modes have a different character. In two-layer

systems having the same density in each layer but different viscosities, fluid inertia is not required to induce interface mode instabilities for cases of negligible interfacial tension. In particular, Loewenherz and Lawrence[11] identify inertialess ($\mathrm{Re}\rightarrow 0$ in each layer) instabilities in cases where the bottom layer viscosity is lower than that of the top layer. In the alternative configuration of lower top layer viscosity, no inertialess interface mode instabilities can be found. Since the surface mode is neutrally stable, inertialess two-layer systems having low top layer viscosities are thus neutrally stable, while those having high top layer viscosities are unstable. Chen[10] explicitly demonstrates how the stability results for the interface mode are altered due to the addition of fluid inertia; furthermore, Chen[2,10] clarifies the relationship to flows confined by two walls, in which fluid inertia is *always* required to obtain interface instabilities. Pozrikidis[12] extends these linear studies by examining the nonlinear evolution of both the confined and free surface configurations.

Although the mechanism is not well understood, Chen[2] points out that the inertialess instability of Loewenherz and Lawrence[11] must be due to the deformability of the free surface and its interaction with the liquid–liquid interface. This emphasizes an important point made by Loewenherz and Lawrence. Although the interface wave modes owe their *existence* to the presence of an interface or free surface, the whole flow field affects each mode. Mathematically, each wave solution is determined as a root of a single characteristic equation that intimately couples the wave modes.

For three-layer flows down an incline, work has focused on the wave motion[9] and linear stability[13,14] at long wavelengths; also, there has been an examination of linear and weakly nonlinear stability and wave propagation for long wavelengths with slightly inclined planes, negligible inertia, and negligible surface and interfacial tensions.[15] Weinstein and Kurz[14] identify an inertialess instability that can be found at zeroth order in wave number, α, in the limit $\alpha \rightarrow 0$; in this limit, all surface tension effects are removed. This instability has a distinctly different character than the two-layer inertialess instability of Loewenherz and Lawrence.[11] A long wavelength examination of the two-layer results of Loewenherz and Lawrence would indicate that instabilities must manifest themselves at $O(\alpha^2)$ or higher to deduce the instability, i.e., *finite* wavelength effects must be included. This is because the two-layer long wavelength analyses of Kao[7,8] indicates that only neutrally stable waves can occur at lowest order in wave number; it is from the $O(\alpha)$ correction, which also brings in the effect of fluid inertia, that the stability is deduced in Kao's work. In the absence of fluid inertia, then, higher orders in wave number must impart the stability characteristics observed by Loewenherz and Lawrence.[11]

An interesting feature of the inertialess long wavelength analysis of Weinstein and Kurz[14] is the mathematical structure of the characteristic equation used to determine the generally complex wave speed, c. The characteristic equation is cubic, has real coefficients, and indicates that the wave propagation is nondispersive. When instabilities arise, then, solutions to the cubic are in the form of a complex conjugate pair, corresponding to interface modes. The conjugate nature of the solutions suggest a strong interaction between the two interface modes, and qualitatively represents a ''resonating'' behavior also seen in three-layer confined flows[16] (see Weinstein and Kurz[14] for further discussion). Despite the fact that the interface modes interact strongly, Weinstein and Kurz[14] show that the air–liquid interface is largely affected by the instability, again emphasizing the global nature of wave propagation as discussed above. Physical configurations that give rise to zeroth-order instability are ones in which the middle layer has a lower viscosity, or density, than those of the adjacent layers; furthermore, the middle layer needs to be thin compared with that of the total thickness of the film, and located toward the center of the three-layer structure. The thin internal layer presumably facilitates the strong interaction required for instability, and the nominally ''symmetrical'' viscosity and density configurations, as well as layer placement, are perhaps intuitively consistent with a mathematical ''symmetry'' required to achieve the complex conjugate behavior discussed above.

Although long wavelength analyses provide some important neutral stability information, waves exhibiting the largest growth typically occur at finite wavelengths that are not accessible via a long wavelength expansion.[11,17] Additionally, while it has been firmly established that long wavelength expansions can be used to deduce the stability of single-layer flows (and hence, the surface mode), the stability of interface modes in multiple-layer systems cannot always be deduced in the long wavelength limit (see, e.g., Fig. 2 of Ref. 17). Chen[10] gives results that show that a system may be stable at long but finite wavelength (*both* surface and interface modes are stable), but unstable at shorter wavelengths; thus, the long wavelength examination of a multiple-layer system may not provide the correct stability conclusion. In practice, it is often the properties of the largest growing wave that are relevant. In an experiment in which all frequencies are given equal amplitudes (i.e., ''white noise''), the observed wave will often be that of the largest growth. Furthermore, in industrial coating processes, waves can be generated via coating die vibrations[18] and flow pulsations at specific frequencies; such disturbances are always

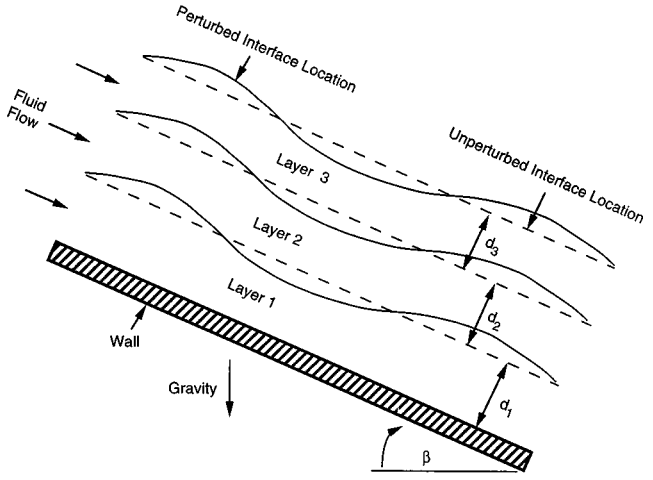

FIG. 1. Geometric configuration of gravity-driven three-layer flow down an inclined plane.

present to some extent in a process. It is the initial amplitude imparted to a wave, coupled with the growth (or decay) of the wave at the given frequency, that determines if the wave amplitude is unacceptable to achieve desired product performance. Although neutral stability is an important characteristic of wave motion, the *magnitude* of the growth (or decay) of wave amplitudes is thus often the practically relevant feature of wave motion.

In this paper, we examine the inertialess wave propagation in three-layer flow down an inclined plane for finite wavelengths. Thus, this work can be viewed as an extension of the previous long wavelength analysis of Weinstein and Kurz,[14] and the three-layer extension of the two-layer study of Loewenherz and Lawrence.[11] We note here that our inertialess analysis provides a physical model for the flow induced on an inclined substrate after coating as discussed above; in a frame of reference moving with the web, the amount of flow induced by gravity in the thin coated film is typically small, and so is the characteristic Reynolds number. We consider configurations where the liquid densities of all layers are the same. Additionally, we assume that the air–liquid interface has surface tension, and all interfacial tensions are zero. These are reasonable assumptions for the typical fluids used in the manufacture of multilayered photographic films. Such fluids are relatively dilute aqueous gelatin solutions with some added emulsions and dispersions; these solutions have solids on the order of 10% or less, yielding relatively small density differences between layers. The miscibility of the layers precludes appreciable interfacial tensions at the liquid–liquid interfaces.

Our results demonstrate that the long-wavelength interface mode instability of Weinstein and Kurz[14] persists into the finite wavelength domain in the form of nearly complex conjugate complex wave speed pairs. The largest growth rate of the instability is orders of magnitude larger than the maximum growth rates identified by Lowenhurz and Lawrence.[11] An additional configuration exhibiting extremely large growth rates, also characterized by nearly complex conjugate behavior, is also identified. The influence of the layer viscosities, thicknesses, and the deformability of the air–liquid interface on the magnitude of the interface mode instabilities is examined.

II. THEORY

Consider the wave propagation problem for three-layer flow down an inclined plane, as sketched in Fig. 1. Here, three Newtonian liquid layers each having density, ρ, are flowing down an infinite plane inclined at angle β under the influence of gravity, g. As indicated in Fig. 1, layer 1 is at the bottom of the three-layer structure, layer 2 is the middle, and layer 3 is the top. The viscosity and specified thickness of each layer are denoted as μ_k and d_k, respectively, where $k \in [1,3]$. We assume that there is a constant surface tension at only the air–liquid interface, denoted as σ, and the liquid–liquid interfacial tensions are assumed to be zero. We denote the total thickness of the three-layer structure as d_T. The origin of the $x-y$ coordinate system is placed at the solid inclined surface (hereafter called the wall), the y axis oriented toward the free surface, and the x axis in the direction of the flow. It is assumed that the dynamics of the air have a negligible effect on the flow. In the unperturbed flow, the fluid interfaces and free surface are all parallel to the wall, and the flow in each layer is everywhere parallel to the wall having a y-dependent velocity field V_{x_k}. In the perturbed flow, waves can form that impart a y component to the velocity field, thickness variations in the liquid layers, and a general $x-y$ dependence for all flow variables. It is assumed that interfacial distortions associated with these waves are small compared with the thickness of their bounding layers; as a result, their propagation characteristics can be accessed via linearization about the unperturbed flow.

The linearized formulation of three-layer flow down an incline under the above assumptions has been developed by Akhtaruzzaman *et al.*,[9] and is reformulated by Weinstein and Kurz.[14] We will generally adhere to the notation and development of Weinstein and Kurz in our work with a few modifications. First, we have chosen to scale appropriate variables

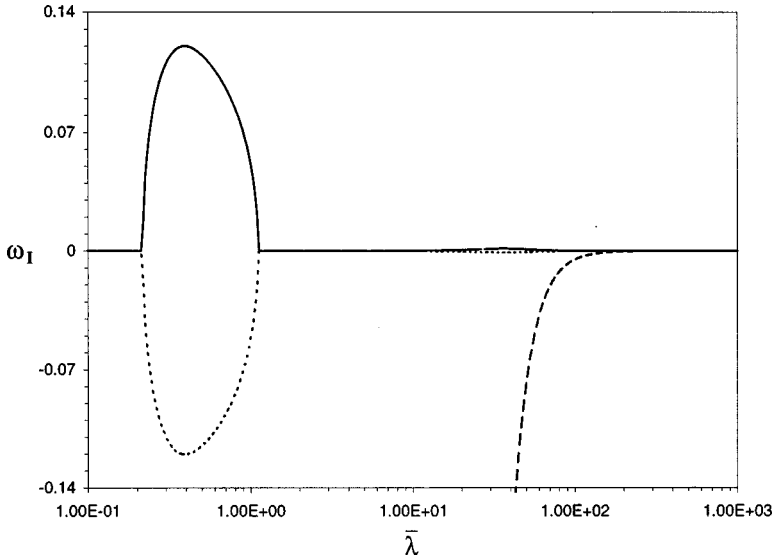

FIG. 2. Plot of growth rate, ω_I, vs wavelength, $\bar{\lambda}$, for a high-viscosity middle-layer configuration. $E_2=5$, $E_3=1$, $\delta_1=\delta_3=0.475$, $\delta_2=0.05$, Ca$=1000$. Interface modes: (—), (···). Surface mode: (– – –). The surface mode is stable at finite wavelengths, and neutrally stable in the long wavelength limit. One of the interface modes is unstable to both short waves and long waves with a neutrally stable band of wavelength in between. The largest growth occurs at the short waves. The two interface modes are nearly complex conjugates for short waves.

using the bottom layer viscosity, μ_1, while Weinstein and Kurz utilize that of the middle layer. Additionally, Weinstein and Kurz generally formulate their three-layer problem for both density and viscosity stratification as well as inertial effects; in this paper, we consider the situation where inertial effects are neglected (i.e., a creeping flow assumption is made) and the densities are the same in each layer.

The unperturbed flow down the inclined plane provides a necessary ''base flow'' for the linearized equations to follow. We define dimensionless variables, denoted with an overbar, as:

$$\overline{V}_{x_k}=\frac{V_{x_k}d_T}{Q_s},\quad \overline{y}=\frac{y}{d_T}, \tag{1a}$$

where a convenient volumetric flow scale, Q_s, is defined as

$$Q_s=\frac{\rho g d_T^3 \sin\beta}{2\mu_1}. \tag{1b}$$

The unperturbed velocity field is parabolic and is given by

$$\overline{V}_{x_k}(\overline{y})=-\frac{1}{E_k}(\overline{y}^2-2\overline{y})+D_k,\quad k\in[1,3], \tag{2a}$$

$$D_k=\sum_{n=1}^{k-1}\left(\frac{1}{E_{n+1}}-\frac{1}{E_n}\right)\left\{\left(\sum_{m=1}^{n}\delta_m\right)^2-2\sum_{m=1}^{n}\delta_m\right\} \tag{2b}$$

and

$$E_k=\frac{\mu_k}{\mu_1},\quad \delta_k=\frac{d_k}{d_T}. \tag{2c}$$

Then, the final functional dependence for $\overline{V}_{x_k}$ is given by

$$\overline{V}_{x_k}=\overline{V}_{x_k}(\overline{y};\delta_2,\delta_3,E_2,E_3), \tag{2d}$$

where by definition,

$$\sum_{n=1}^{3}\delta_n=1;$$

and thus δ_1 is not independent of the other dimensionless thicknesses, i.e.,

$$\delta_1=1-\delta_2-\delta_3. \tag{2e}$$

To examine wave propagation, the time-dependent governing equations and boundary conditions are linearized about the unperturbed flow (2). A stream function is defined for each layer, denoted by $\overline{\Psi}_k Q_s$, and a boundary value problem is obtained solely in terms of $\overline{\Psi}_k$. The solution of linearized equations can be written as the superposition of waves whose translation is characterized by the location, $\overline{x}d_T$, and time, $\overline{t}d_{T^2}/Q_s$, as

$$\overline{\Psi}_k=\phi_k(\overline{y})e^{i(\alpha\overline{x}-\omega\overline{t})}. \tag{3}$$

In (3), $\phi_k(\overline{y})$ is a function to be determined, i denotes imaginary, α is a dimensionless wave number, and ω is a dimensionless frequency. In our examination, we will assume that the growth of waves is temporal; it is thus necessary to determine the complex relation $\omega(\alpha)=\omega_R(\alpha)+i\omega_I(\alpha)$, where α is the purely real wave number defined as $\alpha=2\pi d_T/\lambda$ (λ is the wavelength), and the subscripts R and I denote the real and imaginary parts. The complex dimensionless wave speed, c, is defined as $c=\omega/\alpha$, and is introduced in what follows for convenience.

After substitution of (3) into the linearized system, the following equations and boundary conditions arise in the limit of negligible fluid inertia. The Orr–Somerfeld governing equation arises from the continuity and momentum equations:

$$\frac{d^4\phi_k}{d\overline{y}^4}-2\alpha^2\frac{d^2\phi_k}{d\overline{y}^2}+\alpha^4\phi_k=0,\quad k\in[1,3]. \tag{4a}$$

The no-slip and kinematic boundary conditions at the wall are

$$\phi_1=0, \tag{4b}$$

$$\frac{d\phi_1}{d\overline{y}}=0\quad \text{at } \overline{y}=0, \tag{4c}$$

while the continuity of velocities at each liquid–liquid interface is given by

$$\left.\begin{aligned}&\frac{d\phi_{k+1}}{d\overline{y}}=\frac{d\phi_k}{d\overline{y}}+\left(\frac{\phi_k}{c-\overline{V}_{x_k}}\right)\left[\frac{d\overline{V}_{x_k}}{d\overline{y}}-\frac{d\overline{V}_{x_{k+1}}}{d\overline{y}}\right]\\&\phi_{k+1}=\phi_k\end{aligned}\right\}\ \text{at } \overline{y}=\sum_{n=1}^{k}\delta_n\quad \text{for } k\in[1,2] \tag{4d}$$

(4e)

The normal and tangential components of the dynamic boundary condition at each liquid–liquid interface are expressed as

$$E_k\frac{d^3\phi_k}{d\overline{y}^3}-E_{k+1}\frac{d^3\phi_{k+1}}{d\overline{y}^3}-3\alpha^2\left(E_k\frac{d\phi_k}{d\overline{y}}-E_{k+1}\frac{d\phi_{k+1}}{d\overline{y}}\right)=0\quad \text{at } \overline{y}=\sum_{n=1}^{k}\delta_n \text{ for } k\in[1,2], \tag{4f}$$

$$E_{k+1}\left(\frac{d^2\phi_{k+1}}{d\overline{y}^2}+\alpha^2\phi_{k+1}\right)-E_k\left(\frac{d^2\phi_k}{d\overline{y}^2}+\alpha^2\phi_k\right)=0$$

$$\text{at } \overline{y}=\sum_{n=1}^{k}\delta_n \text{ for } k\in[1,2]. \tag{4g}$$

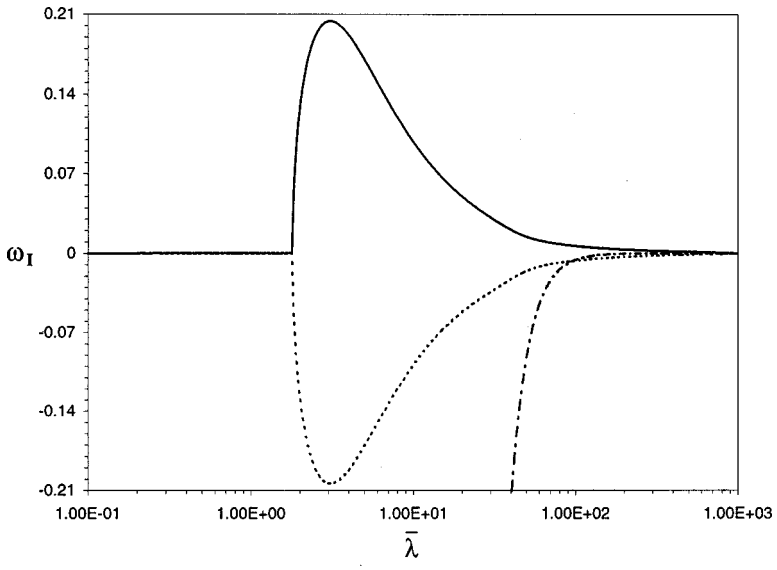

FIG. 3. Plot of growth rate, ω_I, vs wavelength, $\bar{\lambda}$, for a low-viscosity middle-layer configuration. $E_2=0.2$, $E_3=1$, $\delta_1=\delta_3=0.475$, $\delta_2=0.05$, Ca$=1000$. Interface modes: (—), (···). Surface mode: (– – –). The surface mode is stable at finite wavelengths, and neutrally stable in the long wavelength limit. One of the interface modes is unstable when the wavelength exceeds about 2. The largest growth occurs at order one wavelength. The two interface modes are nearly complex conjugates.

At the air–liquid interface, the normal and tangential dynamic boundary condition components are

$$E_3\frac{d^3\phi_3}{d\bar{y}^3}-3\alpha^2E_3\frac{d\phi_3}{d\bar{y}}-i\alpha\left(\frac{\phi_3}{c-\bar{V}_{x_3}}\right)\times\left(2\cot\beta+\frac{\alpha^2}{\mathrm{Ca}}\right)=0 \quad \text{at } \bar{y}=1, \tag{4h}$$

$$E_3\left(\frac{d^2\phi_3}{d\bar{y}^2}+\alpha^2\phi_3\right)-2\left(\frac{\phi_3}{c-\bar{V}_{x_3}}\right)=0 \quad \text{at } \bar{y}=1. \tag{4i}$$

In (4), the capillary number Ca is defined as

$$\mathrm{Ca}=\frac{\mu_1 Q_s}{\sigma d_T}, \tag{4j}$$

where the volumetric flow scale Q_s is given in (1b) and $\bar{V}_{x_k}$ is given by (2). The boundary-value problem (4) constitutes a homogeneous system of equations and boundary conditions, i.e., it is an eigenvalue problem to determine the complex wave speed c as a function of α for given physical, geometrical, and flow properties as

$$c=c(\alpha,\delta_2,\delta_3,E_2,E_3,\cot\beta,\mathrm{Ca}). \tag{5}$$

Corresponding complex eigenfunctions are given by (3), and are dependent on the same constant parameters listed in (5) in addition to the spatial variables.

Equations (4a) can be solved in closed form to obtain the following eigenfunctions:

$$\phi_k=G_k\sinh(\alpha\bar{y})+H_k\cosh(\alpha\bar{y})+I_k\bar{y}\sinh(\alpha\bar{y})+J_k\bar{y}\cosh(\alpha\bar{y}), \quad k\in[1,3], \tag{6}$$

where G_k, H_k, I_k, and J_k are 12 unknown constants. Boundary conditions (4b)–(4i) provide 12 boundary conditions to solve for these constants as well as the complex eigenvalue c. The system can be written in the generalized form

$$\mathbf{A}\eta=c\mathbf{B}\eta, \tag{7}$$

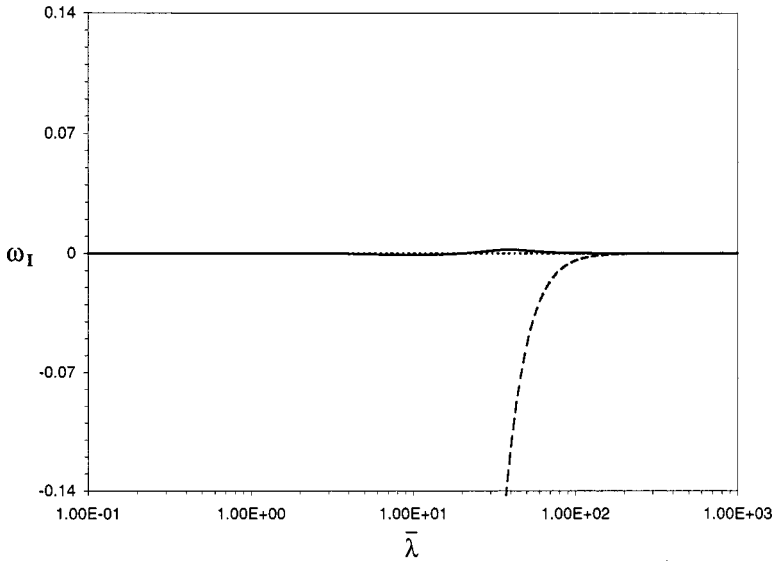

FIG. 4. Plot of growth rate, ω_I, vs wavelength, $\bar{\lambda}$, for a monotonically increasing viscosity configuration. $E_2=5$, $E_3=25$, $\delta_1=\delta_3=0.475$, $\delta_2=0.05$, Ca$=1000$. Interface modes: (—), (···). Surface mode: (– – –). The surface mode is stable at finite wavelengths, and neutrally stable in the long wavelength limit. One of the interface modes is unstable to long wavelength disturbances.

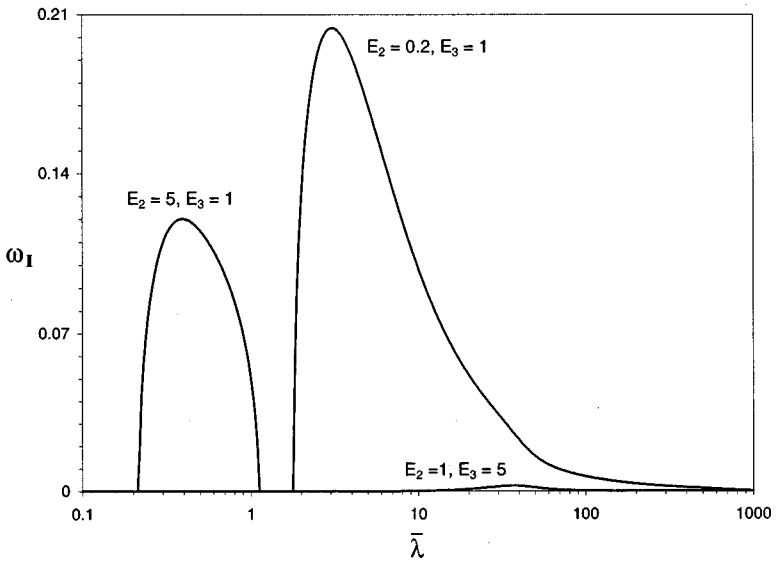

FIG. 5. Comparison of the positive growth rates associated with the nearly complex conjugate modes corresponding to high and low-viscosity middle-layer configurations, and the growth of a typical two-layer long wave instability. The viscosity ratios (E_2, E_3) are marked above each growth rate curve, and $\delta_1 = \delta_3 = 0.475$, $\delta_2 = 0.05$, $\mathrm{Ca} = 1000$. The two-layer results correspond to the plot with $E_2 = 1$, where the bottom and middle layer properties are identical. The three-layer systems have growth rates on the order of 20 times that of the two-layer system.

where η is the vector of the 12 unknown constants, and **A** and **B** are complex 12×12 matrices. Then, once the wave number α is specified for given physical parameters, the generalized complex eigenvalue problem is easily solved to find the complex eigenvalues c and associated eigenvectors η, by utilizing standard techniques of linear algebra. We note here that the 12×12 system can be further reduced to obtain a cubic equation for the complex eigenvalue c. This can be done by using row and column expansions of the determinant of the matrix $\mathbf{A} - c\mathbf{B}$. We used the matrix algorithm to obtain the results provided in this paper as we found the solutions to be more stable than those obtained from the cubic.

The temporal wave growth is quantified by the following exponential term that is extracted from the assumed form (3) as

$$\text{Growth} = e^{\omega_I t}, \tag{8a}$$

where

$$\omega_I = \alpha c_I = \omega_I(\bar{\lambda}, \delta_2, \delta_3, E_2, E_3, \cot\beta, \mathrm{Ca}). \tag{8b}$$

In (8b), c_I is the imaginary part of the complex wave speed whose parameter dependence is given in (5); note that in writing the parameter dependence in (8b), we have replaced the wave number, α, with the dimensionless wavelength, $\bar{\lambda} = 2\pi/\alpha = \lambda/d_T$. From (8), it is clear that when $\omega_I > 0$, wave amplitudes will grow, for $\omega_I < 0$, wave amplitudes will decay, and $\omega_I = 0$ corresponds to neutral stability. The quantity ω_I in (8) is referred to in this paper as the growth rate.

III. RESULTS

There are four possible combinations of viscosity stratification in a three-layer system: monotonically increasing or decreasing from the bottom layer toward the top layer; high-viscosity middle layer; and low-viscosity middle layer. Typical wave growth results for these cases are given in Figs. 2–4 in the form of growth rate, ω_I, as a function of the

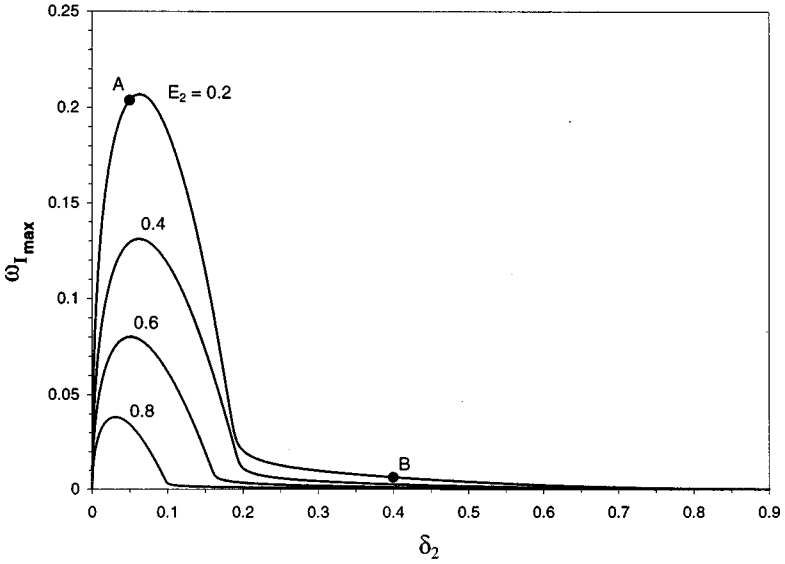

FIG. 6. Maximum growth rate, $\omega_{I_{\max}}$, plotted against the middle-layer depth δ_2, for a variety of viscosity ratios E_2 (low-viscosity middle layer). For this case, $E_3 = 1$, $\delta_1 = \delta_3$, $\mathrm{Ca} = 1000$, and $\beta = 90°$.

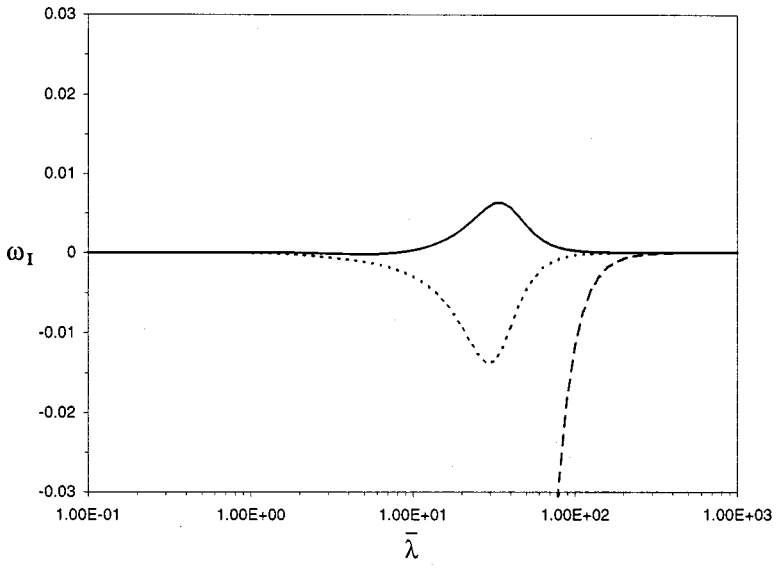

FIG. 7. Plot of growth rate, ω_I, vs wavelength, $\bar{\lambda}$, for the interface and the surface modes corresponding to point B in Fig. 6, where $\delta_2=0.4$. Interface modes: (—), (···). Surface mode: (– – –).

dimensionless wavelength ($\bar{\lambda}=\lambda/d_T$). Note that the parameter dependence of the growth rate is provided by (8). As indicated in Figs. 2–4, a surface mode and two interface mode solutions are obtained for the three-layer systems chosen. Figures 2–4 show that the surface mode is stable at finite wavelengths regardless of the viscosity configuration, and neutrally stable in the limit of infinite wavelength; thus, the surface mode is neutrally stable in the zero Reynolds number limit, in agreement with cited literature results in Sec. I. Thus, the intertialess stability of the three-layer system hinges on the growth of the interface modes. We have found that for all systems having a monotonically decreasing viscosity stratification from the bottom layer to the top, interface modes do not exhibit growth; consequently, the system is neutrally stable in the zero Reynolds number limit. This result is an extension of the two-layer case at zero Reynolds number, which is neutrally stable when the top layer is less viscous.[11,10] For all systems having a monotonically increasing viscosity stratification from the bottom layer to the top, the flow is unstable and has maximum growth rates occurring at long but finite wavelengths such as shown in Fig. 4; the wavelengths and growths are similar in magnitude to those obtained for two-layer flows (a comparison with the two-layer growth results is given in Fig. 5, to be discussed below; see also Ref. 11).

For systems having high-viscosity middle-layer configurations (Fig. 2), it is evident that there are two wavelength regimes in which wave growth may occur. The first regime is characterized by relatively long but finite wavelengths ($\bar{\lambda}\sim 30$); the second regime has shorter waves with wavelengths comparable to the total thickness of the film ($\bar{\lambda}\sim 0.4$). In Fig. 2, the growth rate associated with the longer wavelength instabilities is similar to those found in two-layer configurations with a high viscosity top layer, but the short wavelength growth rates are several orders of magnitude larger. A striking feature of Fig. 2 is the ''mirror-image'' behavior of the wave growth plots for the two interface modes. This behavior arises because the solution of the eigenvalue problem to determine the complex wave speed in

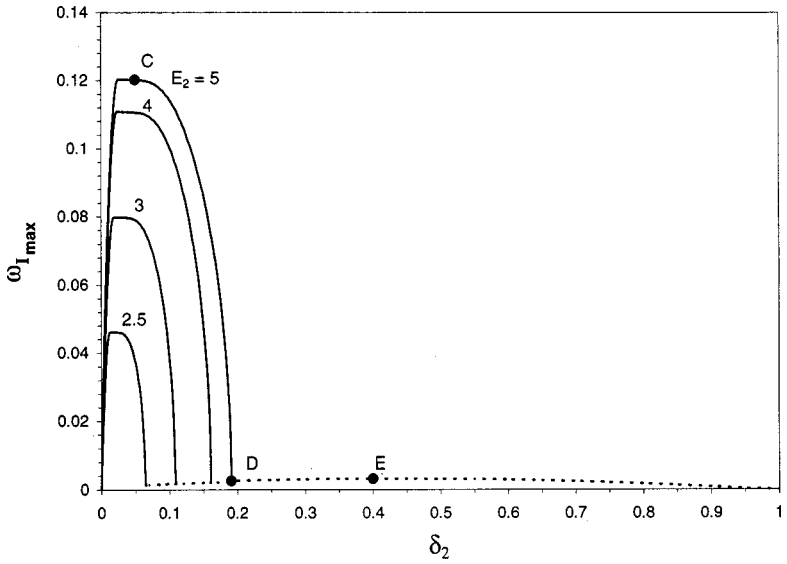

FIG. 8. Maximum growth rate, $\omega_{I_{max}}$, plotted against the middle-layer depth δ_2, for a variety of viscosity ratios E_2 (high-viscosity middle layer). For this case, $E_3=1$, $\delta_1=\delta_3$, Ca=1000, and $\beta=90°$. The dashed line is the locus of points where the longer wavelength instability begins to dominate the wave growth. In reality, each viscosity ratio has a slightly different dashed curve, but they cannot be distinguished on the indicated scale.

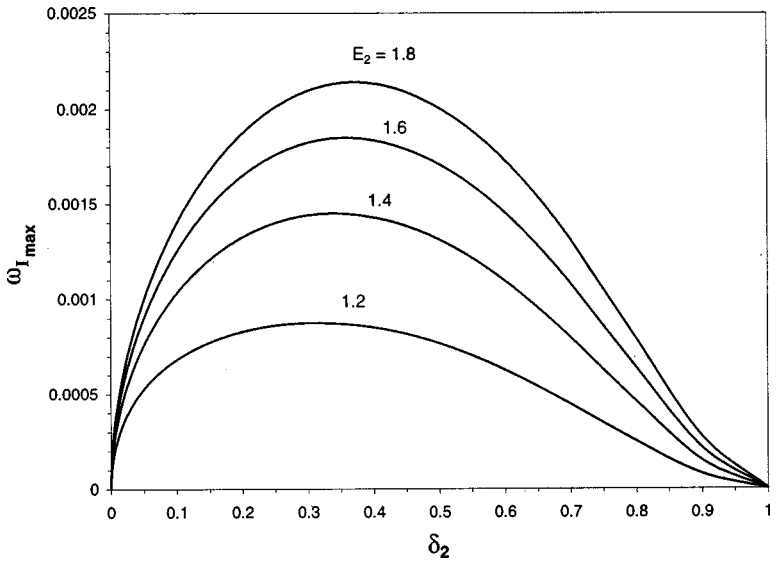

FIG. 9. Maximum growth rate, $\omega_{I_{\max}}$, plotted against the middle-layer depth δ_2, for a variety of viscosity ratios E_2 (high-viscosity middle layer); the viscosity ratios are much smaller than shown in Fig. 8. For this case, $E_3=1$, $\delta_1=\delta_3$. Ca$=1000$, $\beta=90°$.

Sec. II yields nearly complex conjugate solutions for the two interface modes. Note that in Fig. 2, the interface modes are not precisely complex conjugates, but are very close; later in this section, we discuss cases where complex conjugate behavior occurs precisely. Notice that the long wavelength and the much stronger short wave instability are separated by a band of neutrally stable wave numbers in between.

For the low-viscosity middle-layer configuration shown in Fig. 3, the flow is unstable when the wavelength is greater than some critical value. This critical wavelength is also comparable to the total thickness of the film. As in the high-viscosity middle-layer case shown in Fig. 2, the two interface modes in Fig. 3 exhibit nearly complex-conjugate behavior as evidenced by the ''mirror images'' in the growth rate plots. The growth of the disturbances extends all the way to infinitely long waves, without a neutrally stable band of wavelengths as seen in the high-viscosity middle-layer configuration. Note that the long wavelength limit was previously explored by Weinstein and Kurz,[14] who found instabilities when there were low-viscosity middle layers. Thus, the results shown in Fig. 3 can be viewed as the finite wavelength extension of their work. We note that in contrast to the results of Fig. 3, the nearly complex conjugate large growth instability for the high-viscosity middle layer (Fig. 2) does not persist in the long wavelength limit, and is therefore not accessible via a long wavelength expansion; it is thus a new mode of instability not previously identified for three-layer incline flow.

To emphasize the large magnitude of the nearly complex conjugate results of Figs. 2 and 3, a typical comparison of growth rates for a high-viscosity middle-layer, low-viscosity middle-layer, and a two-layer configuration is shown in Fig. 5. Recall that the two-layer case was extensively examined by Loewenherz and Lawrence—Ref. 11. In Fig. 5, we have plotted only the positive growth rates associated with the nearly complex conjugate modes (for the three-layer cases) of Figs. 2 and 3, compared with the growing interface mode instability in the two-layer system (recall that a two-layer flow is unstable only when the bottom layer is less viscous). Clearly, disturbances experience much stronger growth for the high-viscosity middle-layer and the low-viscosity middle-layer configurations as compared to two-layer flows. Furthermore, the maximum growth rates for these two three-layer configurations is achieved at order one wavelengths, while the maximum growth for the two-layer configuration occurs at relatively long (but finite) waves. Note that as indicated in Fig. 5, the high-viscosity middle-layer growth occurs at shorter wavelengths than that associated with low-viscosity middle layers; we have found this result to be typical for film systems that are identical except for the viscosity configuration [i.e., all parameters in (8b) are the same except for E_2 and E_3].

In three-layer systems, relatively large growth rates clearly can arise when there are nearly complex conjugate modes; that is, compared with the relatively small longer wavelength instability, which can arise in two-layer or three-layer systems having monotonically increasing viscosities upwards from the wall (recall that the monotonically decreasing configuration is always stable). The large growth rates of the disturbances in these three-layer flows are due to a strong interaction between the interface modes, i.e., a sort of resonance behavior as described by Weinstein and Kurz.[14] We note here that having a high- or low-viscosity middle layer is necessary, but not sufficient, to achieve the nearly complex conjugate modes that can exhibit large growth; the *magnitude* of the viscosity ratios, as well as the other parameters indicated in (8b), are important. We now explore the parameter conditions under which these large growth modes may arise. To do so, we find it useful to focus on the maximum growth rate (which is always associated with an interface mode as the surface mode is stable) found over the entire wavelength spectrum for a given flow condition. In this way, we can quantify each spectrum, such as shown in Figs. 2–4, with a single number, for the purposes of comparison. When the large growth modes arise, such as in Fig. 2, we are thus focusing on the positive maximum of the nearly complex conjugate curve (e.g., at $\bar{\lambda}\sim 3$ in Fig. 3).

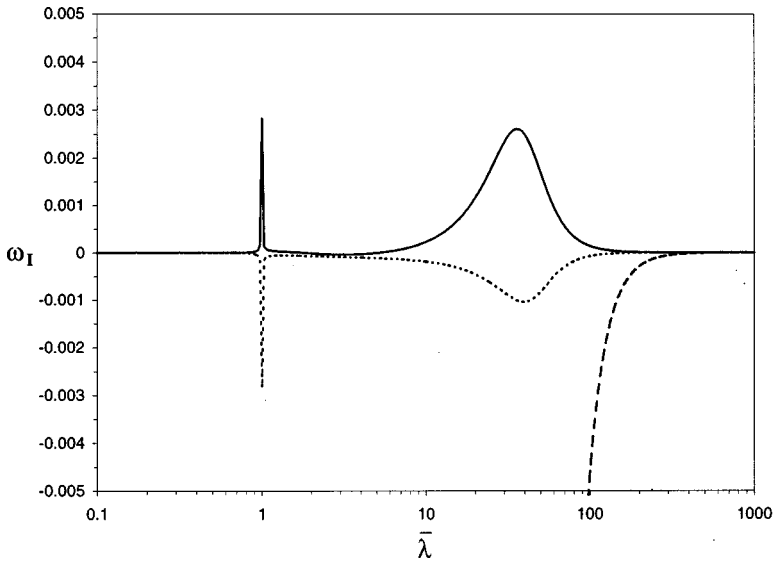

FIG. 10. Plot of growth rate, ω_I, vs wavelength, $\bar{\lambda}$, for the interface and the surface modes corresponding to point D in Fig. 8, where $\delta_2=0.1909$. Interface modes: (—), (···). Surface mode: (– – –). At this value of middle-layer thickness, the long wavelength and short wavelength growths are approximately the same.

We begin by examining the dependence maximum growth rate, denoted as $\omega_{I_{\max}}$, on relative layer thicknesses. We first consider typical results for symmetrically ''sandwiched'' middle layers with the top and the bottom layers having the same viscosity and thickness, $E_3=1$, $\delta_1=\delta_3$. In these calculations, $\mathrm{Ca}=1000$, $\beta=90°$. The maximum growth rate for the low-viscosity middle-layer case is plotted against the middle-layer thickness δ_2 in Fig. 6, for a variety of middle-layer viscosity ratios $E_2(<1)$. It is apparent that there is a maximum in each plot, indicating a most dangerous middle-layer thickness for each viscosity ratio E_2. As E_2 decreases (i.e., the viscosity jump across the middle layer increases) from 0.6 to 0.2, the maximum increases and shifts slightly to larger middle-layer thicknesses, but for these plots, the maximum growth appears when the middle layer is very thin, on the order of $\delta_2\sim 0.05$. As E_2 is increased toward 1, the maximum peak decreases and moves to smaller values of δ_2 (see the curves for $E_2=0.6$, 0.8 in Fig. 6). For $E_2=1$, a single-layer case is recovered (the properties of all layers are identical), and the maximum growth rate is neutrally stable at infinite wavelength (see Figs. 2–4); thus, the case $E_2=1$ corresponds to the δ_2 axis in Fig. 6. For all curves in Fig. 6, it is clear that as $\delta_2\to 0$ or $\delta_2\to 1$, the growth rates decrease to zero; these limits again correspond to a neutrally stable single-layer flow.

There is a dramatic change in the maximum growth rate $\omega_{I_{\max}}$ when the low-viscosity middle-layer thickness δ_2 is increased beyond a certain value, as seen in Fig. 6. For example, for $E_2=0.2$, there is a tenfold decrease in $\omega_{I_{\max}}$ from its peak value when δ_2 is greater than 0.2. This dramatic change in the maximum growth rate $\omega_{I_{\max}}$ is due to a shift of the two interfacial modes from nearly complex conjugate to nonconjugate. This is evident from the spectrums for the representative points A and B on the $\omega_{I_{\max}}$ vs δ_2 plot in Fig. 6. The spectrum for point A is plotted in Fig. 3, where the two interface modes are nearly complex conjugates. As we move along the $E_2=0.2$ curve as δ_2 increases, the two interface modes shift from the nearly complex conjugate behavior at point A ($\delta_2=0.05$), where $\omega_{I_{\max}}$ is about 0.21, to the ob-

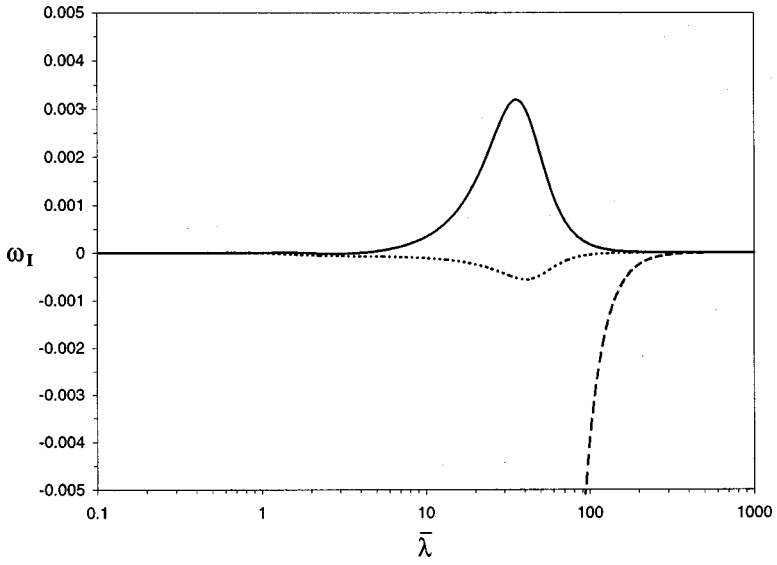

FIG. 11. Plot of growth rate, ω_I, vs wavelength, $\bar{\lambda}$, for the interface and the surface modes corresponding to point E in Fig. 8, where $E_2=5$, $\delta_2=0.4$. Interface modes: (—), (···). Surface mode: (– – –).

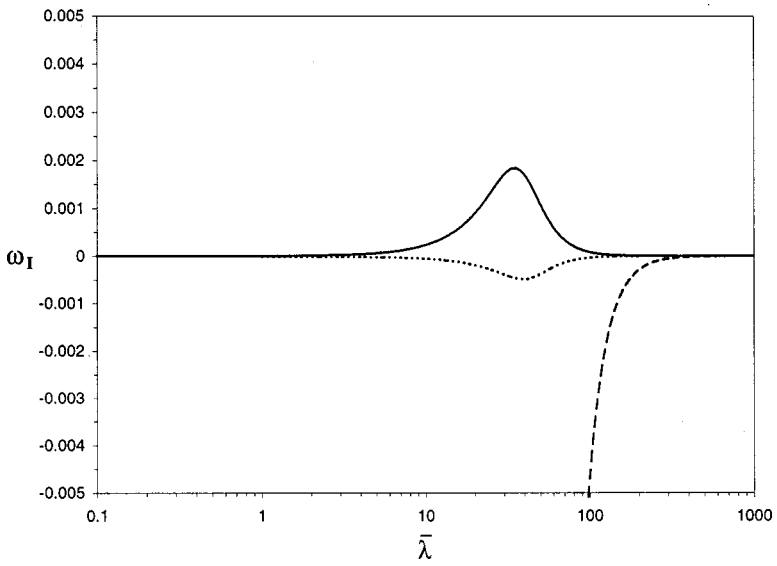

FIG. 12. Plot of growth rate, ω_I, vs wavelength, $\bar{\lambda}$, for the interface and the surface modes for $E_2=1.6$, $\delta_2=0.35$ (where the maximum occurs in Fig. 9) for symmetrically sandwiched case $E_3=1$, $\delta_1=\delta_3$. Interface modes: (—), (···). Surface mode: (– – –). Clearly, there is no mirror-imaging behavior for the interface modes.

viously nonconjugate behavior at point B ($\delta_2=0.4$, Fig. 7) where $\omega_{I_{\max}}$ drops to about 0.01. Thus, a very thin symmetrically sandwiched low-viscosity middle layer results in a pair of nearly complex conjugate interface modes, which gives large growth rate.

We now examine cases of symmetrically ''sandwiched'' middle layers having high viscosities ($E_2>1$); as above, the top and the bottom layers have the same viscosity and thickness ($E_3=1,\delta_1=\delta_3$) where Ca$=1000$ and $\beta=90°$. Figures 8 and 9 show the dependence of the maximum growth rate on middle-layer thickness, δ_2, for a variety of middle-layer viscosity ratios, $E_2(>1)$. Figure 8 shows that there is a most dangerous middle-layer thickness for which a maximum growth is achieved; for cases of $E_2=4,5$, this maximum occurs at $\delta_2\sim 0.05$. As the viscosity ratio is reduced to $E_2=2.5$, the magnitude of the maximum growth peak is reduced and simultaneously shifts to smaller middle-layer thicknesses. This behavior is precisely as in the low-viscosity middle-layer case shown in Fig. 6.

There is a dramatic drop-off of the maximum growth rate $\omega_{I_{\max}}$ in each of the curves in Fig. 8. This drop is associated with a shift of the maximum growth from short waves to long waves. To illustrate this, we use the curve $E_2=5$ as an example. The spectra for the growing interface mode are plotted against the wavelength $\bar{\lambda}$ for each of the representative points *C*, *D*, and *E*. The spectrum for the growing interface mode for point *C* is given in Fig. 2, where it is seen that there are two peaks, one occurring at a short wavelength and the other occurring at a very long wavelength. The peak at the short wavelength is orders of magnitude larger than the peak at the long wavelength. As we move along the $E_2=5$ curve in Fig. 8 toward point *D*, $\omega_{I_{\max}}$ is reduced and the short wavelength peak is subsiding while the long wavelength peak is growing. At point *D*, $\delta_2=0.1909$, and the long wavelength peak has grown large enough to have comparable magnitude as the short wavelength peak (Fig. 10). For values of δ_2 slightly greater than that of point *D*, the short wavelength peak disappears. This is indicated in the spectrum associated with point *E*, $\delta_2=0.4$, where we have a purely long wave instability (Fig. 11). Thus, for the high-viscosity middle-layer cases, the dramatic variation of the maximum growth rate $\omega_{I_{\max}}$ with the middle-layer thickness δ_2 reflects a shift from short to long wave instability. This is in contrast to the low-viscosity middle-layer case where such a change is associated with a change from nearly complex conjugate growth to nonconjugate growth.

It is noted that for smaller viscosity ratios (the value of E_2 is less than 2.1), there is no such dramatic drop-off of the maximum growth rate $\omega_{I_{\max}}$ when the middle-layer thickness δ_2 is increased (Fig. 9). Figure 9 gives analogous results to those in Fig. 8, except for viscosity ratios $E_2\leqslant 1.8$. Note the distinctly different curve shapes in Fig. 9 compared with Fig. 8, as well as the small magnitude of the wave growth. For the indicated viscosity ratios in Fig. 9, nearly complex conjugate modes do not arise, and the long wavelength instability having wave growth comparable to that of two-layer systems dominates (see the spectrum for $E_2=1.6$ in Fig. 12). The shorter wavelength instability associated with nearly complex conjugate modes becomes dominant for $E_2>2.1$. Therefore, one can conclude that for the high-viscosity middle-layer configuration, large growth of the interface mode occurs only when the viscosity ratio is large (in the example examined above, $E_2>2.1$) and the middle-layer thickness δ_2 is small ($\delta_2<0.2$ for the example examined).

We now turn our attention to the asymmetrically sandwiched thin middle layers with a fixed middle-layer thickness δ_2. The top and the bottom layers have the same viscosities, $E_3=1$, but may have different thickness. The middle layer can be placed at various locations as the bottom-layer thickness δ_1 is varied. In Fig. 13, the maximum growth rate $\omega_{I_{\max}}$ is plotted against the bottom layer thickness δ_1 for a thin middle-layer $\delta_2=0.05$ with various viscosity ratios $E_2<1$ (low-viscosity middle layers). It is interesting to note that $\omega_{I_{\max}}$ reaches a maximum when the bottom layer takes about 40%–50% of the total thickness. This means that the maximum in $\omega_{I_{\max}}$ occurs when the middle layer is almost symmetrically sandwiched (δ_3 is close to

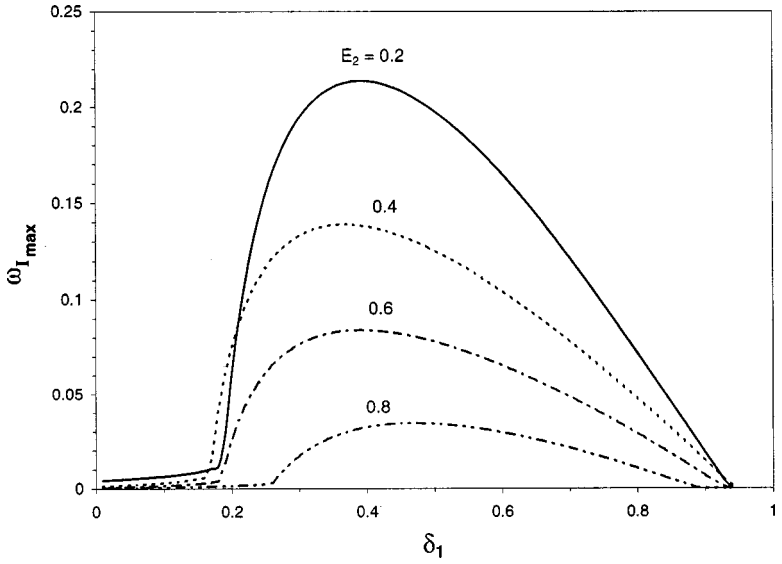

FIG. 13. Maximum growth rate, $\omega_{I_{\max}}$, plotted against the bottom-layer depth δ_1, for a variety of viscosity ratios E_2 (low-viscosity middle layer). For this case, $E_3=1$, $\delta_2=0.05$, Ca$=1000$, and $\beta=90°$.

δ_1). On the other hand, when the middle layer has a higher viscosity, $E_2>1$, the maximum in $\omega_{I_{\max}}$ often occurs when the bottom layer is thinner than the top layer, as is evident in Fig. 14.

With the thickness and viscosity effects explored in (8b), we now examine the influence of the capillary number, Ca, on wave growth. The capillary number is a measure of the deformability of the free surface. In the large surface tension limit, Ca$\to 0$, the free surface is nondeformable. On the other hand, the free surface becomes very flexible when surface tension is zero, i.e., Ca$\to\infty$. The effect of surface deformability on wave growth is demonstrated in Figs. 15 and 16. For these calculations, the layer structure is in a symmetrically ''sandwiched'' configuration with the top and the bottom layers having the same viscosity and thickness: $E_3=1$, $\delta_1=\delta_3=0.475$, $\delta_2=0.05$, and $\beta=90°$. Figure 15 provides data for low-viscosity middle-layer cases $E_2<1$, and Fig. 16 provides data for high-viscosity middle-layer cases $E_2>1$. When $E_2=1$ in these plots, all three layers have the same viscosity (i.e., a single-layer flow is achieved) and the maximum growth rate is zero. As E_2 is decreased from unity, as seen in Fig. 15 for the low-viscosity middle-layer configuration, the maximum growth rate increases as the inverse capillary number Ca^{-1} is increased. This indicates that deformability of the free surface is reducing the growth rate for the low-viscosity middle-layer configuration. A distinguished feature of Fig. 15 is that the maximum growth rate becomes insensitive to the capillary number when Ca$^{-1}<0.4$ or Ca$^{-1}>50$. Furthermore, the maximum growth rate approaches different limits for the nondeformable free surface limit Ca$^{-1}\to\infty$, and the flexible limit Ca$^{-1}\to 0$. The limit of nondeformable surface can be deduced by inspection of the system (4). The deformability of the free surface is incorporated via the term $\phi_3/(c-\overline{V}_{x_3})$ in (4h) and (4i). In the limit as Ca$^{-1}\to\infty$, Eq. (4h) reduces to $\phi_3=0$ at the free surface, and the deformability term is thus lost in (4i). As a result, the matrices **A** and **B** in (7) are purely real, and matrix/row reductions of the determinant of $\mathbf{A}-c\mathbf{B}$ yield a quadratic equation. Then, if wave growth arises [i.e., c is complex in (7)],

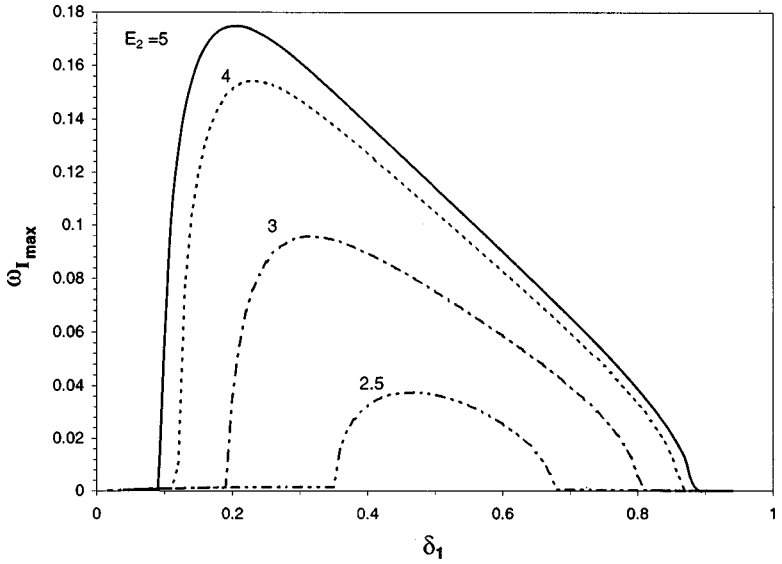

FIG. 14. Maximum growth rate, $\omega_{I_{\max}}$, plotted against the bottom-layer depth δ_1, for a variety of viscosity ratios E_2 (high-viscosity middle layer). For this case, $E_3=1$, $\delta_2=0.05$, Ca$=1000$, and $\beta=90°$.

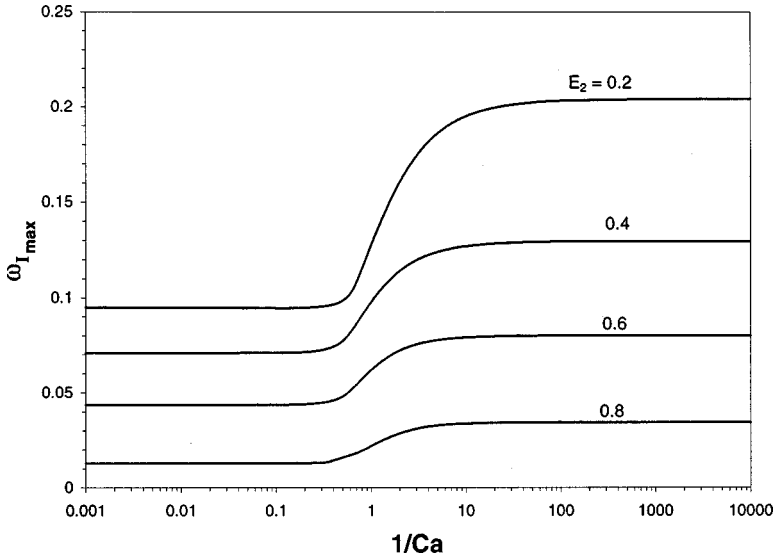

FIG. 15. Maximum growth rate, $\omega_{I_{max}}$, vs inverse capillary number, 1/Ca, for symmetrically sandwiched low-viscosity middle-layer configurations, $E_3=1$. The middle-layer viscosity ratio E_2 is varied and marked above each curve. $\delta_1=\delta_3=0.475$, $\delta_2=0.05$.

complex conjugate modes must be present. For the high-viscosity middle-layer case ($E_2>1$) shown in Fig. 16, we see that the maximum growth rates increase with increased values of E_2, as expected from previous figures. As indicated in Fig. 16, the maximum growth rate has a maximum at some intermediate capillary number for $E_2=1.4,1.8$. For these cases, note that short wavelength nearly complex conjugate modes do not arise (see Figs. 9 and 12). For $E_2=2.5$, nearly complex conjugate modes exist for all indicated data; in contrast to the situation where $E_2<1$ in Fig. 15, the maximum growth rate decreases with increased Ca^{-1}. Additionally, as the value of E_2 is increased to 3.0 and above, the maximum growth rates (which are associated with the nearly conjugate modes) become flat, independent of the capillary number. A physical explanation for this phenomenon is lacking, but we noticed that when E_2 reaches 3 and beyond, the wavelength corresponding to the maximum growth rate remains unchanged as the capillary number is varied over the wide range considered here.

The incline angle β, which incorporates the effect of hydrostatic pressure gradient, appears only in a single parameter, $2\cot\beta+\alpha^2/\mathrm{Ca}$, found in Eq. (4h). Therefore, a decrease in the incline angle β is equivalent to an increase in surface tension (i.e., a decrease in the capillary number Ca) for any given wave number α. Thus, variations of the maximum growth rate $\omega_{I_{max}}$ with the incline angle can be easily deduced from the $\omega_{I_{max}}$ vs Ca curves for the case of $\beta=90°$ in Figs. 15 and 16.

IV. SUMMARY AND CONCLUSIONS

In this paper, we have examined the effect of viscosity stratification on wave propagation in three-layer flow down an inclined plane at vanishingly small Reynolds number and at finite wavelengths, for cases of negligible liquid–liquid interfacial tensions. We have found that the long-wavelength interface mode instability of Weinstein and Kurz[14] persists into the finite wavelength domain in the form of nearly com-

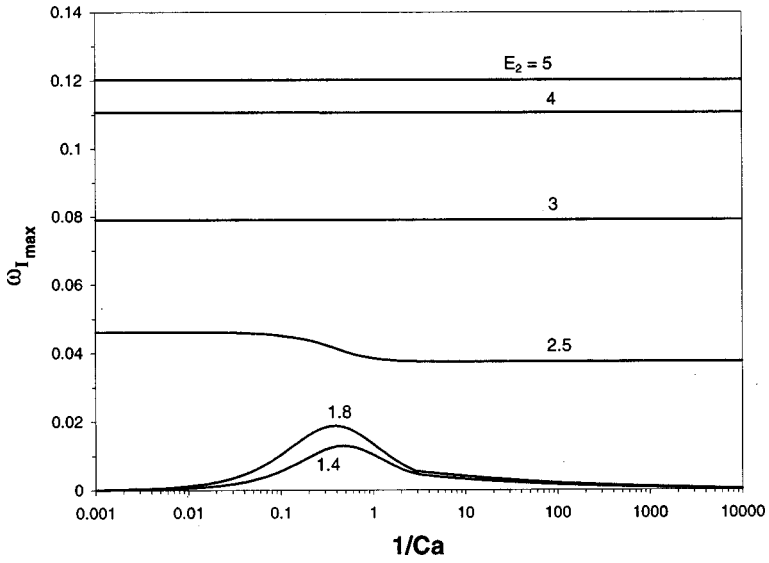

FIG. 16. Maximum growth rate, $\omega_{I_{max}}$, vs inverse capillary number, 1/Ca, for symmetrically sandwiched high-viscosity middle-layer configurations where $E_3=1$. The middle-layer viscosity ratio E_2 is varied and marked above each curve. $\delta_1=\delta_3=0.475$, $\delta_2=0.05$.

plex conjugate wave speed pairs. As in the case of Weinstein and Kurz,[14] the physical configuration necessary to achieve instability are a low-viscosity and thin internal layer with respect to the other layers in the film. When this layer is nominally centrally located in the film, the maximum growth rates are achieved. The largest growth rates of the instability are found at finite wavelengths on the order of the total thickness of the film, and are orders of magnitude larger than the maximum growth rates identified by Lowenhurz and Lawrence[11] for two-layer inertialess flows. We have also found additional configurations exhibiting extremely high growth rates, also characterized by nearly complex conjugate behavior, that are not accessible via a long or short wavelength asymptotic limit. These three-layer structures have thin, high-viscosity internal layers, the largest growth rates typically being found with the internal layer displaced off-center toward the bottom of the film. The characteristic wavelengths associated with largest growth are on the order of ten times smaller than those for the low-viscosity internal layer cases.

The influence of the deformable free surface on the growth of these nearly complex conjugate *interface* modes has been studied and found to be significant. Indeed, it is the free surface deformability that accounts for why the interface modes are, in general, not precisely complex conjugates; it is only in the limit of infinite surface tension, i.e., a nondeformable interface, that precisely complex conjugate solutions may arise. At finite surface tensions, i.e., finite capillary numbers as shown in Fig. 15, the influence of the air–liquid interface on interface mode growth rates can be significant. The three-layer results of this paper thus serve to further reinforce the comments of Loewenherz and Lawrence,[11] who point out that although interface modes may have a local character (in that they owe their existence to the presence of jumps in viscosity in the film) the global nature of the flow field affects the growth of the waves. Mathematically, this is evidenced by the fact that the dispersion relations for the surface and interface modes are obtained simultaneously as the solution of the eigenvalue system (7), and are thus inherently coupled.

[1] D. D. Joseph and Y. Y. Renardy, *Fundamentals of Two Fluids Dynamics* (Springer, New York, 1992).
[2] K. P. Chen, ''Interfacial instabilities in stratified shear flows involving multiple viscous and viscoelastic fluids,'' Appl. Mech. Rev. **48**, 763 (1995).
[3] T. B. Benjamin, ''Wave formation in laminar flow down an inclined plane,'' J. Fluid Mech. **2**, 554 (1957).
[4] C. S. Yih, ''Stability of liquid flow down an inclined plane,'' Phys. Fluids **6**, 321 (1963).
[5] J. M. Floryan, S. H. Davis, and R. E. Kelly, ''Instabilities of a liquid film flowing down a slightly inclined plane,'' Phys. Fluids **30**, 983 (1987).
[6] D. R. Woods and S. P. Lin, ''Critical angle of shear wave instability in a film,'' Trans. ASME, J. Appl. Mech. **63**, 1051 (1996).
[7] T. W. Kao, ''Role of the interface in the stability of stratified flow down an inclined plane,'' Phys. Fluids **8**, 2190 (1965).
[8] T. W. Kao, ''Role of viscosity stratification in the stability of two-layer flow down an incline,'' J. Fluid Mech. **33**, 561 (1968).
[9] A. F. M. Akhtaruzzaman, C. K. Wang, and S. P. Lin, ''Wave motion in multilayered liquid films,'' Trans. ASME, J. Appl. Mech. **45**, 25 (1978).
[10] K. P. Chen, ''Wave formation in the gravity-driven low-Reynolds number flow of two liquid films down an incline,'' Phys. Fluids A **5**, 3038 (1993).
[11] D. S. Loewenherz and C. J. Lawrence, ''The effect of viscosity stratification on the stability of a free surface flow at low Reynolds number,'' Phys. Fluids A **1**, 1686 (1989).
[12] C. Pozrikidis, ''Gravity-driven creeping flow of two adjacent layers through a channel and down a plane wall,'' J. Fluid Mech. **371**, 345 (1998).
[13] C. K. Wang, J. J. Seaborg, and S. P. Lin, ''Instability of multi-layered liquid films,'' Phys. Fluids **21**, 1669 (1978).
[14] S. J. Weinstein and M. R. Kurz, ''Long-wavelength instabilities in three-layer flow down an incline,'' Phys. Fluids A **3**, 2680 (1991).
[15] I. L. Kliakhandler and G. I. Sivashinsky, ''Viscous damping and instabilities in stratified liquid film flowing down a slightly inclined plane,'' Phys. Fluids **9**, 23 (1997).
[16] C. H. Li, ''Instability of three-layer viscous stratified flow,'' Phys. Fluids **12**, 2473 (1969).
[17] S. J. Weinstein, ''Wave propagation in the flow of shear-thinning fluids down an incline,'' AIChE. J. **36**, 1873 (1990).
[18] S. J. Weinstein, J. M. Baumlin, and J. Servant, ''The propagation of surface waves in flow down an oscillating inclined plane,'' AIChE. J. **39**, 1113 (1993).